

Non-local interference in arrival time

Ali Ayatollah Rafsanjani,^{1,*} MohammadJavad Kazemi,^{2,†} Vahid Hosseinzadeh,³ and Mehdi Golshani³

¹*Department of Physics, Sharif University of Technology, Tehran, Iran*

²*Department of Physics, Faculty of Science, University of Qom, Qom, Iran*

³*School of Physics, Institute for Research in Fundamental Sciences (IPM), P.O. Box 19395-5531, Tehran, Iran*

Although position and time have different mathematical roles in quantum mechanics, with one being an operator and the other being a parameter, there is a space-time duality in quantum phenomena; Many phenomena observed in the spatial domain are also observed in the temporal domain. In this context, we propose a modified version of the two double-slit experiment using entangled atoms to observe a non-local interference in the arrival time distribution. Our numerical simulations demonstrate a complementary relationship between the one-particle and two-particle interference visibility in the arrival time distribution, which is analogous to the complementary relationship observed in the arrival position distribution. To overcome the complexities of computing the arrival time distribution in quantum mechanics, we employ a Bohmian treatment. Our approach to investigating this experiment can be applied to a wide range of phenomena, and it appears that the predicted non-local temporal interference and associated complementarity relationship are universal behaviors of entangled quantum systems that may manifest in various phenomena.

PACS numbers: 03.65.Ta, 05.10.Gg

I. INTRODUCTION

In quantum theory, several effects that were initially observed in the spatial domain have subsequently been observed in the time domain. These effects include a wide range of phenomena such as diffraction in time [1–4], interference in time [5–8], Anderson localization in time [9, 10] and several others [11–13]. To extend this line of research, we propose a simple experimental setup that can be used to observe a *non-local interference in arrival time*, which is analogous to the non-local interference in arrival position observed in entangled particle systems [14–20].

The proposed experimental setup involves two double-slit arrangement in which a source emits pairs of entangled atoms toward slits [17, 21]. Such entangled atoms can be produced, for example, via a four-wave mixing process in colliding Bose-Einstein condensates [22, 23]. The atoms fall due to the influence of gravity and then they reach horizontal fast single-particle detectors, which record the arrival time and arrival position of the particles, as depicted in Fig. 1. In fact, a similar arrangement had previously been proposed for observing non-local two-particle interference in arrival *position* distribution [17]. The critical difference between our setup and theirs is that the slits in our setup are not placed at the same height. This leads to height-separated wave packets that spread in space during falling and overlap each other. Moreover, we do not consider the horizontal screens at the same height, so the particles may be detected at completely different timescales. Our study indicates that these apparently small differences lead to significant interference in the two-particle arrival time

distribution, which did not exist in the previous versions of the experiment. This phenomenon is experimentally observable, thanks to the current single-atom detection technology. Our numerical study shows that the required space-time resolution in particle detection is achievable using current single-atom detectors, such as the recent delay-line detectors described in [23, 24] or the detector used in [25, 26].

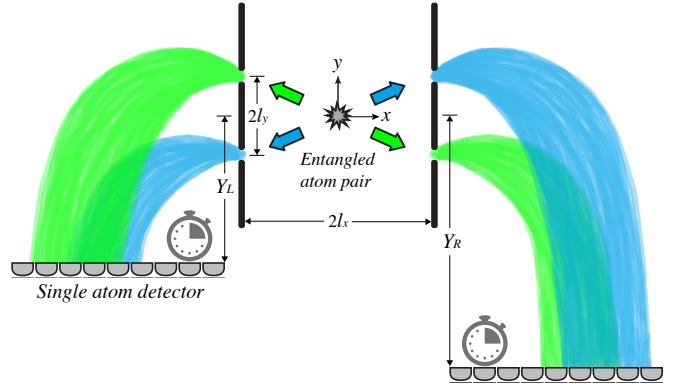


FIG. 1. A schematic representation of the double-double-slit setup. The source emits pairs of entangled particles, each of which passes through a double-slit and then has a free fall. Two arrays of fast particle detectors are considered, on both sides, recording the detection events. The Y_L , Y_R , $2l_y$ and $2l_x$ represent the vertical distance between the left detection screen and origin, the vertical distance between the right detection screen and right slits, the vertical distance between slits and the horizontal distance between slits, respectively.

The theoretical analysis of the proposed experiment is more complex than that of the usual double-double-slit experiment due to at least two reasons. Firstly, since the two particles are not observed simultaneously, the wave function of the two particles collapses to a single-particle

* aliayat@physics.sharif.edu

† kazemi.j.m@gmail.com

wave function at the time the first particle is detected in the middle of the experiment. Secondly, the theoretical analysis of arrival time distribution is more complex than that of arrival position distribution. This is because, in the mathematical framework of orthodox quantum mechanics, position is represented by a self-adjoint operator, while time is just treated as a parameter [27]. As a result, the Born rule cannot be directly applied to the time measurements. This fact, coupled with other issues such as the quantum Zeno paradox [28, 29], leads to some ambiguities in calculating the arrival time distribution [30–36]. In fact, there is no agreed-upon method for calculating the arrival time distribution, although several different proposals have been put forth based on various interpretations of quantum theory [37–47].

Most of the arrival time distribution proposals are limited to simple cases, such as a free one-particle in one dimension, and are not yet fully extended to more complex situations, such as our double-double-slit setup. Nevertheless, the Bohmian treatment seems suitable for analyzing the proposed setup since it can be unambiguously generalized for multi-particle systems in the presence of external potentials. Thus, in this paper, we investigate the proposed experiment using recent development in the Bohmian arrival time for entangled particle systems, including detector back-effect [20, 46]. The results could contribute to a better understanding of the non-local nature of quantum mechanics in the time domain. Moreover, beyond the proposed setup, our theoretical approach has potential applications in related fields such as atomic ghost imaging [23, 48], and in state tomography via time-of-flight measurements [26, 49, 50].

The structure of this paper is as follows: In Section II, we introduce the theoretical framework and the numerical results. Then, in Section III, we discuss the physical insights of the results, including signal locality and the complementarity between one-particle and two-particle interference visibility. In Section IV, we study the screen back-effect, and then we summarize our results in Section V.

II. THEORETICAL FRAMEWORK

Bohmian mechanics, also known as pilot wave theory, is a coherent realistic version of quantum theory, which avoids the measurement problem [51, 52]. In the Bohmian interpretation, in contrast to the orthodox interpretation, the wave function does not give a complete description of the quantum system. Instead, the actual trajectories of particles are taken into account as well, and this can provide a more intuitive picture of quantum phenomena [53]. Nonetheless, it has been proved that in the quantum equilibrium condition [54, 55], Bohmian mechanics is experimentally equivalent to orthodox quantum mechanics [56, 57] *insofar as the latter is unambiguous* [58–60]; e.g., in usual position or momentum measurements at a specific time. In recent years, Bohmian

mechanics has gained renewed interest for various reasons [61–64]. One of these reasons is the fact that Bohmian trajectories can lead to clear predictions for quantum characteristic times, such as tunneling time duration [65, 66] and arrival time distribution [20, 38, 59].

Here, we investigate the proposed double-double slit setup using Bohmian tools. According to Bohmian Mechanics, the state of a two-particle system is determined by the wave function $\Psi(\mathbf{r}_1, \mathbf{r}_2)$ and particles' actual positions $(\mathbf{R}_1, \mathbf{R}_2)$. The time evolution of the wave function is given by a two-particle Schrödinger equation

$$i\hbar \frac{\partial}{\partial t} \Psi_t(\mathbf{r}_1, \mathbf{r}_2) = \sum_{i=1,2} \frac{\hbar^2}{2m_i} \nabla_i^2 \Psi_t + V_i(\mathbf{r}_i) \Psi_t, \quad (1)$$

which in the proposed setup $V_i(\mathbf{r}_i) = -m_i \mathbf{g} \cdot \mathbf{r}_i$ and \mathbf{g} represents gravitational field. The particle dynamics is given by a first-order differential equation in configuration space, the "guidance equation",

$$\frac{d}{dt} \mathbf{R}_i(t) = \mathbf{v}_i^{\Psi_t}(\mathbf{R}_1(t), \mathbf{R}_2(t)), \quad (2)$$

where $\mathbf{v}_i^{\Psi_t}$ are the velocity fields associated with the wave function Ψ_t ; i.e. $\mathbf{v}_i^{\Psi_t} = (\hbar/m_i) \Im(\nabla_i \Psi_t / \Psi_t)$ [67]. When the particle 1, for example, is detected at time $t = t_c$, the two-particle wave function collapses *effectively* to a one-particle wave function, i.e. as $\Psi_{t_c}(\mathbf{r}_1, \mathbf{r}_2) \rightarrow \psi_{t_c}(\mathbf{r}_2)$, where [68, 69],

$$\psi_{t_c}(\mathbf{r}_2) = \Psi_{t_c}(\mathbf{R}_1(t_c), \mathbf{r}_2), \quad (3)$$

which is known as the "conditional wave function" in Bohmian formalism [67, 70]. For $t > t_c$, the time evolution of the wave function is given by following the one-particle Schrödinger equation

$$i\hbar \frac{\partial}{\partial t} \psi_t(\mathbf{r}_2) = \frac{-\hbar^2}{2m_2} \nabla_2^2 \psi_t(\mathbf{r}_2) + V_2(\mathbf{r}_2) \psi_t(\mathbf{r}_2), \quad (4)$$

and the remaining particle motion is determined by the associated one-particle guidance equations

$$\frac{d}{dt} \mathbf{R}_2(t) = \mathbf{v}_2^{\psi_t}(\mathbf{R}_2(t)), \quad (5)$$

It is important to note that, in general, a conditional wave function does not obey the Schrödinger equation [71]. However, in a measurement situation, the interaction of the detected particle with the environment (including the detection screen) cancels any entanglement between undetected and detected particles, due to the decoherence process [72]. Therefore, in this situation, after the measurement process, the conditional wave function represents the "effective wave function" of the undetected particle [71, 73], which satisfies the one-particle Schrödinger equation [46, 71].

We focus our study on the propagation of the wave function from the slits to the detection screens. Thus,

we may consider the initial wave function as follows [74–76]:

$$\Psi_{t_0}(\mathbf{r}_1, \mathbf{r}_2) = N \left[\left(\frac{1-\eta}{2} \right) \Psi_{t_0}^{(\times)}(\mathbf{r}_1, \mathbf{r}_2) + \left(\frac{1+\eta}{2} \right) \Psi_{t_0}^{(\parallel)}(\mathbf{r}_1, \mathbf{r}_2) \right],$$

in which N is a normalization constant,

$$\begin{aligned} \Psi_{t_0}^{(\times)}(\mathbf{r}_1, \mathbf{r}_2) &= [g_u^+(\mathbf{r}_1)g_d^-(\mathbf{r}_2) + g_d^+(\mathbf{r}_1)g_u^-(\mathbf{r}_2)] + 1 \leftrightarrow 2, \\ \Psi_{t_0}^{(\parallel)}(\mathbf{r}_1, \mathbf{r}_2) &= [g_u^+(\mathbf{r}_1)g_u^-(\mathbf{r}_2) + g_d^+(\mathbf{r}_1)g_d^-(\mathbf{r}_2)] + 1 \leftrightarrow 2, \end{aligned}$$

and

$$\begin{aligned} g_u^\pm(x, y) &= G(x; \sigma_x, \pm l_x, \pm u_x)G(y; \sigma_y, +l_y, +u_y), \\ g_d^\pm(x, y) &= G(x; \sigma_x, \pm l_x, \pm u_x)G(y; \sigma_y, -l_y, -u_y), \end{aligned}$$

where G is a Gaussian wave function

$$G(x; \sigma, l, u) = Ne^{-(x-l)^2/4\sigma^2 + imu(x-l)/\hbar}.$$

The Gaussian-type initial wave function is a minimal toy model which is commonly used in the literature (e.g., see [18, 19, 42, 75–80]). The parameter η controls the entanglement of the wave function. It is easy to see that $\eta = 0$ leads to a separable state, whereas $|\eta| = 1$ leads to a maximally entangled state; for $\eta = +1$ the state is maximally correlated, and for $\eta = -1$ the state is maximally anticorrelated [75]. We also have symmetrized the wave function, as we have considered the particles as indistinguishable Bosons. It is worth noting that even without using the slits, this kind of initial wave function could be produced and reliably controlled using optical manipulation [81, 82] of an entangled state generated from colliding Bose-Einstein condensates [22, 23, 83]. Furthermore, since the free two-particle Hamiltonian is separable, the time evolution of this wave function can be found from eq.(1) analytically as

$$\Psi_t(\mathbf{r}_1, \mathbf{r}_2) = N \left[\left(\frac{1-\eta}{2} \right) \Psi_t^{(\times)}(\mathbf{r}_1, \mathbf{r}_2) + \left(\frac{1+\eta}{2} \right) \Psi_t^{(\parallel)}(\mathbf{r}_1, \mathbf{r}_2) \right]$$

in which functions $\Psi_t^{(\times)}(\mathbf{r}_1, \mathbf{r}_2)$ and $\Psi_t^{(\parallel)}(\mathbf{r}_1, \mathbf{r}_2)$ are constructed out of time dependent Gaussian wave functions G_t as in (6) where

$$\begin{aligned} G_t(x; \sigma, l, u, a) &= (2\pi s_t^2)^{-\frac{1}{4}} e^{i\frac{ma}{\hbar}lt} e^{[-(x-l-ut-ax^2/2)^2]} \\ &\times e^{i\frac{m}{\hbar}[(u-at).(x-l-\frac{ut}{2})-a^2t^3/6]} \end{aligned} \quad (6)$$

and $s_t = \sigma(1 + i\frac{t\hbar}{2m\sigma^2})$ [84]. Using this wave function, the detection time and position of the first observed particle are uniquely determined by solving Eq. 2. Then, using Eq. 5, we can find the trajectories of the remaining particles after the first particle detection.

Using trajectories, we can find the joint detection data distribution in $(t_L, x_L; t_R, x_R)$ space where $t_{L/R}$ is the detection time, and $x_{L/R}$ is the detection position on the

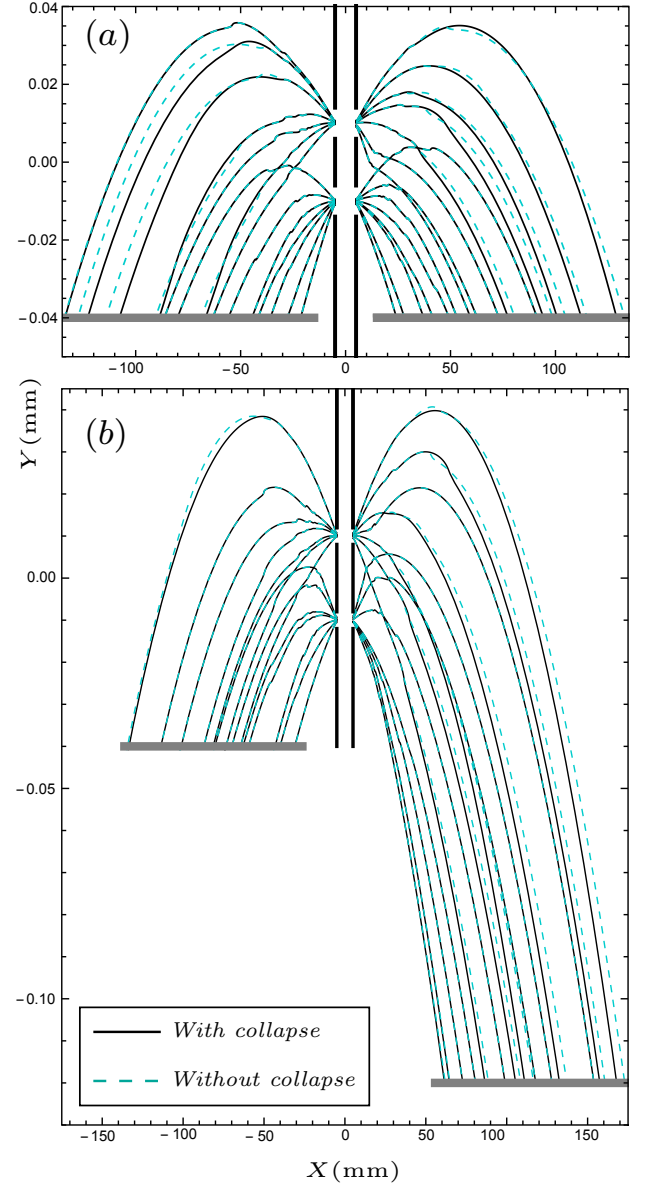


FIG. 2. The effect of collapse on trajectories. The cyan curves represent the case without considering collapse and the black ones are the modified trajectories due to the collapse effect. One can see that the right black trajectories gradually deviate from green ones as the left screen detects the particle. In panel (a) the screens are placed at the same height, while in panel (b) they are located at different heights.

left/right screen. The probability density behind this distribution can be formally written as

$$\begin{aligned} P(t_L, x_L; t_R, x_R) &= \int d\mathbf{R}^0 |\Psi_0(\mathbf{R}^0)|^2 \\ &\times \prod_{i=L, R} \delta(t_i - T_i(\mathbf{R}^0)) \delta(x_i - X_i(\mathbf{R}^0)), \end{aligned}$$

where $T_{L,R}(\mathbf{R}_1^0, \mathbf{R}_2^0)$ and $X_{L,R}(\mathbf{R}_1^0, \mathbf{R}_2^0)$ are the arrival

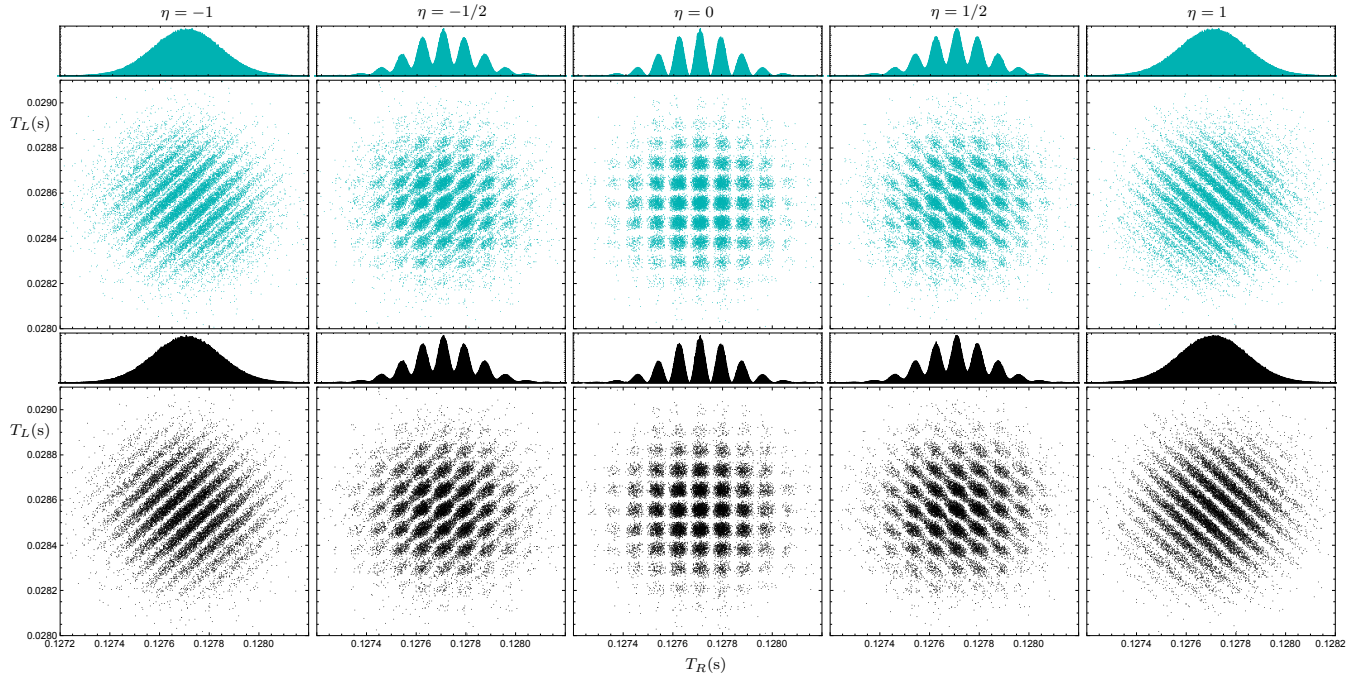


FIG. 3. Two-particle interference patterns of sodium atoms for different entanglement levels η , with and without wave function collapse. The upper and lower scatter plots in each panel show the joint distributions of arrival times to the horizontal screens for the cases without (dark cyan) and with (black) collapse, respectively. The histograms in each panel show the marginal distributions of arrival times to the right screen at $Y_R = -8$ cm. The left screen is at $Y_L = 4$ mm. The slit distance is $20\mu\text{m}$, the initial wave packet widths are $1\mu\text{m}$, and the initial horizontal velocity is 20 m/s .

time and position of the particle with initial condition $(\mathbf{R}_1^0, \mathbf{R}_2^0)$ to the left and right screen, respectively. Note, how the above joint distribution and, therefore, any marginal distribution out of it, is sensitive to the Bohmian dynamics through functions T and X and also to the Born rule by $|\Psi_0(\mathbf{R}^0)|^2$. The joint two-particle arrival time distribution is then defined as,

$$\Pi(t_L, t_R) = \int \int P(t_L, x_L; t_R, x_R) dx_L dx_R. \quad (7)$$

The right and left marginal arrival time distributions are also defined correspondingly as,

$$\begin{aligned} \Pi_L(t_L) &= \int P(t_L, t_R) dt_R \\ \Pi_R(t_R) &= \int P(t_L, t_R) dt_L. \end{aligned}$$

The trajectories of the particles and the resulting arrival time distributions are numerically computed for an ensemble of particles whose initial positions are sampled from $|\Psi|^2$, and the corresponding results are described in the next section.

III. RESULTS

In numerical studies of this work, the parameters of the setup have been chosen as $\sigma_x = \sigma_y = 10^{-6}\text{ m}$, $u_x = 20$

m/s , $u_y = 0$, $l_x = 5 \times 10^{-3}\text{ m}$, $l_y = 10^{-5}\text{ m}$. These values are in agreement with the proposed setup in reference [85] in which colliding helium-4 atoms have been considered for producing an initial entangled state [86]. However, we consider heavier atom pairs as well, which lead to a more visible interference pattern for some values of parameters and the locations of the screens—See Fig. 5.

In Fig. 2, for Helium atoms, some of Bohmian trajectories are plotted. In this figure, the cyan trajectories are without considering the collapse effect and the black ones are with that. One can see that after the detection of the left particle, the right particle starts to deviate from the cyan trajectories as the conditional wave function now guides it. It is worth noticing that, the ensemble of trajectories can be experimentally reconstructed using weak measurement techniques [18, 87, 88], which can be used as a test of our result.

In Figs. 3 and 4, the joint arrival time distribution $\Pi(t_L, t_R)$ and also the right and left marginal distributions $\Pi_R(t_R)$ and $\Pi_L(t_L)$ are plotted, for cesium atoms in two cases: with collapse effect in black and without that in dark-cyan. Fig. 3 shows the one-particle and two-particle temporal interference pattern for fixed screens' locations and different values of the entanglement parameter η . The marginal distributions are generated using 10^6 trajectories. However, for clarity, only 10^4 points are shown in the joint scatter plots. As mentioned, maximum entanglement occurs when $|\eta| = 1$ and when $\eta = 0$,

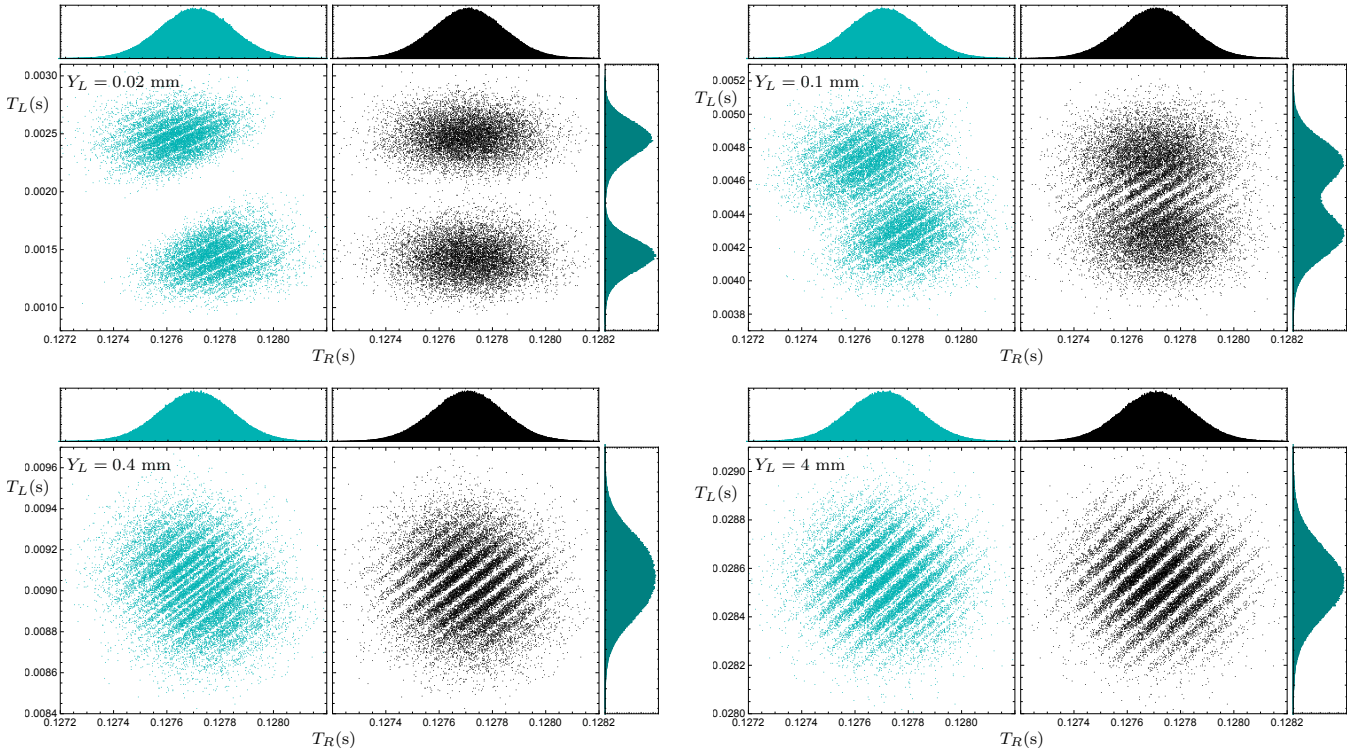


FIG. 4. Arrival time distributions of sodium atoms in the double-double slit experiment, with and without wave function collapse. The left and right scatter plots in each panel show the joint distributions of arrival times to the horizontal screens for the cases without (dark cyan) and with (black) collapse, respectively. The upper and right histograms in each panel show the marginal distributions of arrival times to the right and left screens, respectively. The slit distance is $20 \mu\text{m}$, the initial wave packet widths are $1 \mu\text{m}$ in both directions, the initial horizontal velocity is 20 m/s , and the initial vertical velocity is zero. The right screen is 8 cm below the slit center.

the particles are entirely uncorrelated. As one can see in Fig. 3, the visibility of the joint and marginal distributions have an inverse relation. This behavior represents a *temporal* counterpart to the complementarity between the one-particle and two-particle interference visibilities of the arrival *position* pattern, which can be observed in the conventional double-slit experimental configuration [75, 77, 89]. Moreover, the correction of the two-particle distributions due to the collapse effect decreases with the turning off of the entanglement, and in $\eta = 0$, interference patterns with and without correction are the same. In fact, in this case, we have $\Pi(t_L, t_R) = \Pi_R(t_R)\Pi_L(t_L)$.

In Fig. 4, the one-particle and two-particle temporal interference patterns for different positions of the left screen is depicted, while the entanglement parameter fix to $\eta = -1$. The difference between patterns is obvious in the cases without collapse effect consideration (dark-cyan plots) and by including the effect (black plots). The closer the left screen is to the slits, the earlier the wave function reduction occurs, and its effect is more visible on the joint distribution. Note that, despite the fact that the collapse effect changes particles' trajectories and resulting joint distribution, this effect did not change the one-particle distribution patterns. This shows the establishment of the no-signaling condition, despite the manifest

non-local Bohmian dynamics: The right marginal arrival time distribution, as a local observable quantity, turns out to be independent of whether there is any screen on the left or not, and if there is any, it is not sensitive to the location of that detection screen. Note that this fact is not trivial because the well-known no-signaling theorem is proved for observable distributions provided by a POVM. However, in the general case, the *intrinsic* Bohmian arrival time distribution cannot be described by a POVM, at least when the detector back-effect is ignored [33, 90]. In the next section, we discuss more on the detector back-effect.

IV. DETECTOR BACK-EFFECT

The arrival distributions computed in the previous sections should be considered as *ideal* or *intrinsic* distributions [90], since the influence of the detector is ignored in our theoretical manner. Such an idealization is commonly used in most previous studies of Bohmian arrival time distribution (for example, see [6, 59, 90–93]), and seems more or less to be satisfactory in many applications including the double-slit experiment [50, 87, 94]. Nonetheless, in principle, the presence of the detector

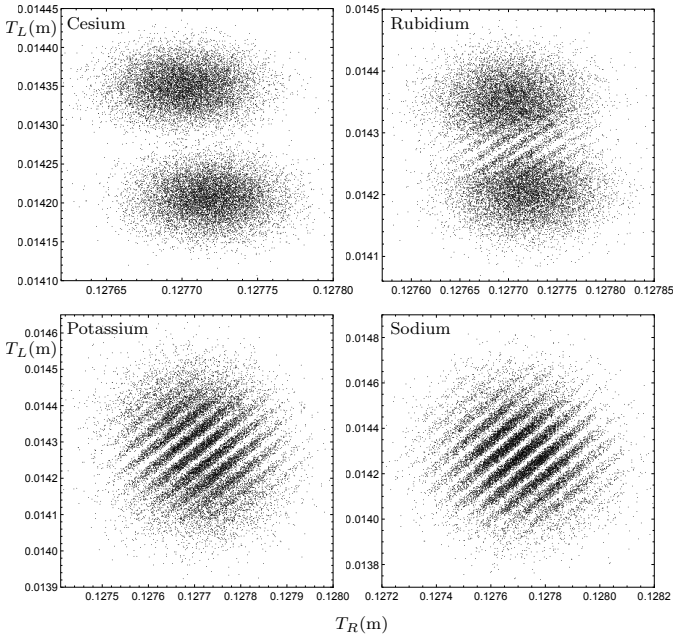


FIG. 5. Joint distributions of arrival times to the horizontal screens for different elements with different masses. The right and left screens are at 8 cm and 1 mm from the slit center, respectively. The slit distance is 20 μm , the initial wave packet widths are 1 μm , the initial velocity is 20 m/s, and the gravitational acceleration is 9.81 m/s².

could modify the wave function evolution, even before the particle detection [95]. This is called the detector back-effect. To have a more thorough investigation of detection statistics, we should consider this effect. However, due to some fundamental problems, such as measurement problem and the quantum Zeno effect [28], a complete investigation of the detector effects is problematic at the fundamental level, and it is less obvious how to model an ideal detector [30, 31, 95]. Nonetheless, some phenomenological non-equivalent models are proposed, such as the generalized Feynman path integral approach in the presence of an absorbing boundary [96–99], Schrödinger equation with a complex potential [100], Schrödinger equation with absorbing (or complex Robin) boundary condition [46, 100–103], and so on. In this section, we merely consider the absorbing boundary rule (ABR), which is compatible with the Bohmian picture and recently developed for multi-entangled particle systems [46]. The results of other approaches may not be the same [47]—See also Appendix VI. So a detailed study of the differences is an interesting topic, which is left for future works.

A. Absorbing Boundary Rule

According to the ABR, the particle wave function ψ evolves according to the free Schrödinger equation, while

the presence of a detection screen is modeled by imposing the following boundary conditions on the Detection screen, $\mathbf{x} \in \mathbb{S}$,

$$\mathbf{n} \cdot \nabla \psi = i\kappa \psi, \quad (8)$$

where $\kappa > 0$ is a constant characterizing the type of detector, in which $\hbar\kappa/m$ represents the momentum that the detector is most sensitive to. This boundary condition ensures that waves with wave number κ are completely absorbed while waves with other wave numbers are partly absorbed and partly reflected [102, 104]. Note that, The Hille-Yosida theorem implies that the Schrödinger equation with above boundary condition has a unique solution for every initial wave function defined on one side of the boundary.

The boundary condition (8), implies that Bohmian trajectories can cross the boundary \mathbb{S} only outwards and so there are no multi-crossing trajectories. In the Bohmian picture, a detector clicks when and where the Bohmian particle reaches detection surface \mathbb{S} . In fact, it is a description of a “hard” detector, i.e., one that detects a particle immediately when it arrives at the surface \mathbb{S} . Nonetheless, it should be noted that the boundary absorbs the particle but not completely the wave. The wave packet moving towards the detector may not be entirely absorbed, but rather partially reflected [102].

The application of absorbing boundary condition in arrival time problem was first proposed by Werner [101], and recently it is re-derived and generalized by other authors using various methods [46, 100, 102, 103]. Especially, it is recently shown that in a suitable (non-obvious) limit, the imaginary potential approach yields the distribution of detection time and position in agreement with the absorbing boundary rule [100]. Moreover, Dubey, Bernardin, and Dhar [103] have shown that the ABR can be obtained in a limit similar but not identical to that considered in the quantum Zeno effect, involving repeated quantum measurements. Recently the natural extension of the absorbing boundary rule to the n -particle case is discussed by Tumulka [46]. The key element of this extension is that, upon a detection event, the wave function gets collapsed by inserting the detected position, at the time of detection, into the wave function, thus yielding a wave function of $(n - 1)$ particles. We use this formalism for the investigation of detector back-effect in our double-double-slit setup.

B. Numerical Results

In our experimental setup, due to the influence of gravity, the reflected portions of the wave packets return to the detector screen, while some of them are absorbed and some are reflected again. This cycle of absorption and reflection is repeated continuously. The associated survival probabilities are plotted in Fig. 7 for some values of detector parameter, $\kappa = \kappa_0, 2\kappa_0, 3\kappa_0, \kappa_0/3$, where the κ_0 is defined using classical estimation of particles momentum

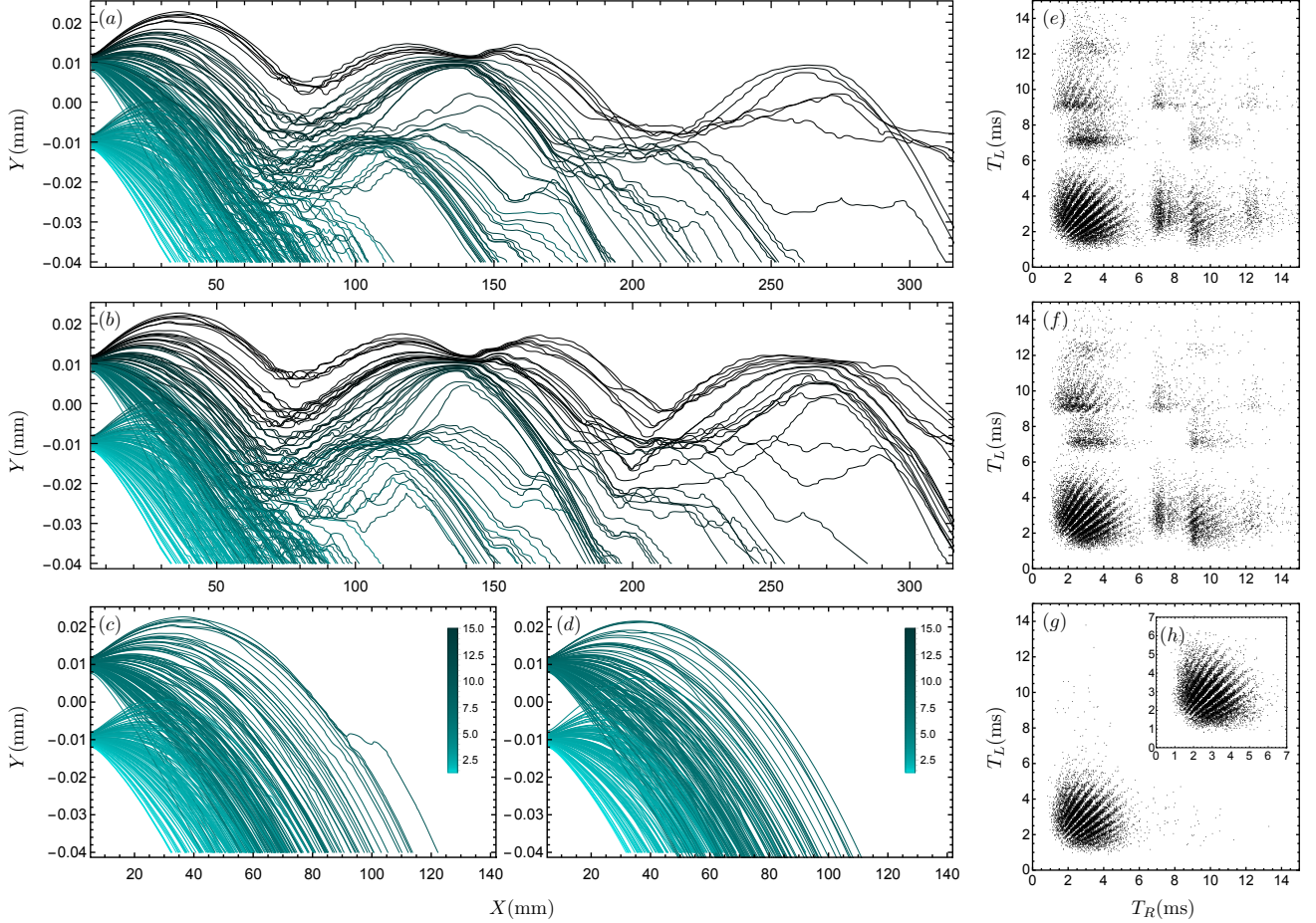


FIG. 6. Bohmian trajectories and joint arrival time distributions of helium atoms in the two double-slit setup, with different detector characterizing constants κ . The detectors are placed at $Y_R = Y_L = -40\mu\text{m}$ and have an absorbing boundary. The slit distance is $20\mu\text{m}$, the initial wave packet widths are $1\mu\text{m}$ in both directions, and the initial velocities are $u_x = 20\text{ m/s}$ and $u_y = 0$. The panels (a), (b), and (c) show the trajectories for $\kappa = 3\kappa_0$, $\kappa = \kappa_0/3$, and $\kappa = \kappa_0$, respectively. The panel (d) shows the trajectories without the detector back-effect, only truncated at the detector position. The panels (e), (f), (g), and (h) show the corresponding joint distributions of arrival times to the horizontal screens.

at the screen as $\kappa_0 = m\sqrt{2gY_R}/\hbar$. The corresponding Bohmian trajectories and arrival time distributions are presented in Fig. 6. As one can see in Figs. 7 and 6, when $\kappa = \kappa_0$, most of the trajectories are absorbed, and approximately none of them are reflected, which is similar to the case when the detector back effect is ignored. These results show that, at least for the chosen parameters, when we use a proper detector with $\kappa = \kappa_0$, the ideal arrival time distribution computed in the previous section, without considering the detector back effect, produces acceptable results. However, in general, Figs. 7 and 6 show that the detector back effect cannot be ignored and it leads to new phenomena: i.e., a "fractal" of the interference pattern.

V. SUMMARY AND OUTLOOK

In this work, we proposed a double-double-slit setup to observe non-local interference in the arrival time of entangled particle pairs. Our numerical study shows a complementarity between one-particle visibility and two-particle visibility in the arrival time interference pattern, which is very similar to the complementarity observed for the arrival position interference pattern [75]. Moreover, the results of our study indicate that arrival time correlations can serve as an entanglement witness, thereby suggesting the potential use of temporal observables for tasks related to quantum information processing [105, 106].

As noted in the introduction, the theoretical analysis of the suggested experiment is more complex than that of a typical double-slit experiment due to several connected fundamental problems, including the arrival time problem, the measurement problem, and the quantum

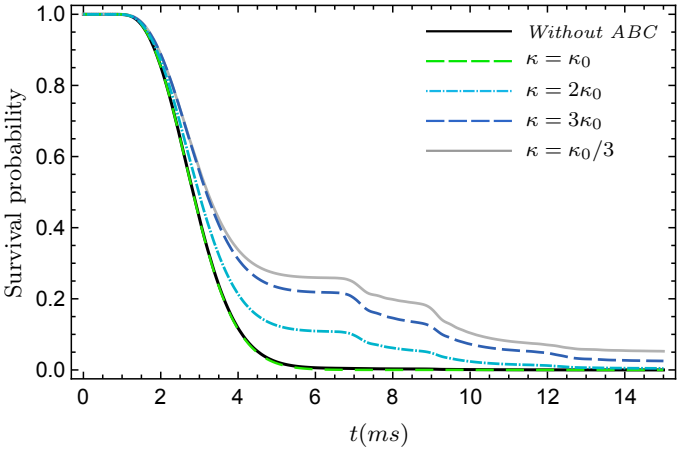


FIG. 7. Survival probability of helium atoms in the two double-slit setup, with different detector characterizing constants κ . The atoms are subject to gravity and are absorbed by the detectors with an absorbing boundary. The setup parameters are the same as in Fig. 6.

Zeno paradox. We use a Bohmian treatment to circumvent these problems. Our approach can be used for a more accurate investigation of various phenomena beyond the double-double-slit experiment, such as ghost imaging [23], Hong–Ou–Mandel Effect [107], temporal state tomography [49], and so on, which are usually analyzed in a semi-classical approximation (see Appendix VI).

It is worth noting that, based on other interpretations of quantum theory, there are other non-equivalent approaches that can, in principle, be used to investigate the suggested experiment [45, 47]. However, these approaches need to be extended for entangled particle systems first. Comparing the results obtained by these various approaches can be used to test the foundations of quantum theory. Specifically, it appears that measuring the arrival time correlations in entangled particle systems can sharply distinguish between different approaches to the arrival time problem [106]. A more detailed investigation of this subject is left for future works.

VI. APPENDIX: SEMI-CLASSICAL ANALYSIS

Despite the absence of an agreed-upon fundamental approach for arrival time computation, a semiclassical analysis is routinely used to analyze observed data. This approach is often sufficient, especially when particle detection is done in the far-field regime [33, 84]. In this analysis, it is assumed that particles move along classical trajectories, and the arrival time distribution is computed using the quantum initial momentum distribution [90, 108, 109]. It is important to compare the semiclassical analysis with our Bohmian result. To this end, we re-derive the semiclassical approximation and extend it

to the near-field regime, using the Wigner phase-space formalism.

The Wigner distribution function is defined as follows [110]:

$$f^W(\mathbf{r}, \mathbf{p}) = \frac{1}{\sqrt{2\pi\hbar}} \int \Psi^*(\mathbf{r} - \mathbf{y}) \Psi(\mathbf{r} + \mathbf{y}) e^{i\mathbf{p}\cdot\mathbf{y}} d^4y.$$

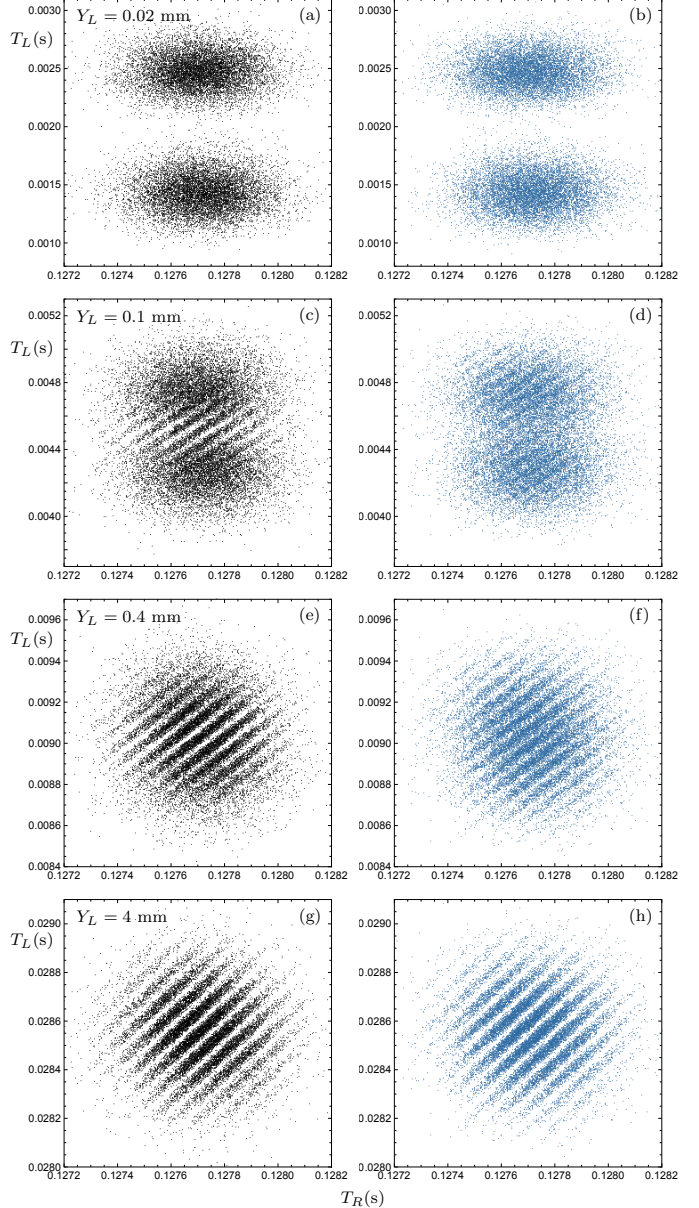


FIG. 8. Joint distributions of arrival times to the horizontal screens for sodium atoms in the two double-slit experiment, with semiclassical and Bohmian analysis, for different left screen positions. The left scatter plots show the Bohmian patterns with the wave function collapse effect (black), and the right scatter plots show the semiclassical patterns without the collapse effect (dark blue). The right screen is at $Y_R = -8$ cm, the slit distance is $20\mu\text{m}$, the initial wave packet widths are $1\mu\text{m}$, and the initial horizontal velocity is 20 m/s .

where $\mathbf{r} = (\mathbf{r}_1, \mathbf{r}_2)$, $\mathbf{y} = (\mathbf{y}_1, \mathbf{y}_2)$ and $\mathbf{p} = (\mathbf{p}_1, \mathbf{p}_2)$. The marginals of this distribution function are quantum position and momentum distributions [110]. The Schrodinger equation leads to the following quantum Liouville equation for Wigner distribution function [111],

$$\frac{\partial f_t^W}{\partial t} + \sum_{i=1,2} \frac{\mathbf{p}_i}{m} \cdot \nabla_{\mathbf{x}_i} f + \nabla_{\mathbf{p}_i} \cdot (f \mathbf{F}_i^W) = 0 \quad (9)$$

By comparing this equation with the classical Liouville equation, the Wigner trajectories are defined as follows [111, 112]

$$\frac{d^2 \mathbf{x}_i}{dt^2} = \frac{\mathbf{F}_i^W}{m} \quad (10)$$

These trajectories are used to understand various quantum phenomena [113–120][121]. For a constant external gravitational force, this equation of motion leads to the trajectories exactly the same as classical trajectories. Moreover, due to the non-overlapping of the initial

Gaussian wave packets, the Wigner formalism leads to the following initial (positive) phase-space distribution.

$$f_{t_0}^W(\mathbf{r}_1, \mathbf{r}_2; \mathbf{p}_1, \mathbf{p}_2) \approx |\Psi_{t_0}(\mathbf{r}_1, \mathbf{r}_2)|^2 |\tilde{\Psi}_{t_0}(\mathbf{p}_1, \mathbf{p}_2)|^2, \quad (11)$$

where $\tilde{\Psi}_{t_0}(\mathbf{p}_1, \mathbf{p}_2)$ is wave function in momentum space. Using the initial phase space distribution and classical (or Wigner) trajectories, we compute the arrival time distribution in our setup. In Figure 8, the semi-classical joint arrival time distribution is compared with the corresponding Bohmian result. As can be seen in this figure, when the left screen is in the near-field or far-field, the semi-classical distributions are more or less the same as the Bohmian distributions (see the panels (a) and (b) of Fig. 8 for near-field, and the panels (g) and (h) for far-field). However, in the middle-field, i.e., the panels (c)–(f) of Fig. 8, the Bohmian distribution is distinguishable from the semi-classical approximation. This determines an important window in the parameter space of this experiment, which can be used to test Bohmian predictions and other arrival time proposals in a strict manner.

[1] M. Moshinsky, *Physical Review* **88**, 625 (1952).

[2] Č. Brukner and A. Zeilinger, *Physical Review A* **56**, 3804 (1997).

[3] A. Goussev, *Physical Review A* **87**, 053621 (2013).

[4] R. Tirole, S. Vezzoli, E. Galiffi, I. Robertson, D. Maurice, B. Tilmann, S. A. Maier, J. B. Pendry, and R. Sapienza, *Nature Physics* , 1 (2023).

[5] P. Sriftgiser, D. Guéry-Odelin, M. Arndt, and J. Dalibard, *Physical Review Letters* **77**, 4 (1996).

[6] M. M. Ali and H.-S. Goan, *Journal of Physics A: Mathematical and Theoretical* **42**, 385303 (2009).

[7] T. Kaneyasu, Y. Hikosaka, S. Wada, M. Fujimoto, H. Ota, H. Iwayama, and M. Katoh, *Scientific Reports* **13**, 6142 (2023).

[8] F. J. Rodriguez-Fortuño, *Nature Physics* , 1 (2023).

[9] K. Sacha, *Scientific reports* **5**, 10787 (2015).

[10] K. Sacha and D. Delande, *Physical Review A* **94**, 023633 (2016).

[11] L. A. Hall, S. Ponomarenko, and A. F. Abouraddy, *Optics Letters* **46**, 3107 (2021).

[12] P. Coleman, *Nature* **493**, 166 (2013).

[13] P. Ryczkowski, M. Barbier, A. T. Friberg, J. M. Dudley, and G. Genty, *Nature Photonics* **10**, 167 (2016).

[14] D. M. Greenberger, M. A. Horne, and A. Zeilinger, *Physics Today* **46**, 22 (1993).

[15] D. Strekalov, A. Sergienko, D. Klyshko, and Y. Shih, *Physical review letters* **74**, 3600 (1995).

[16] C. Hong and T. Noh, *JOSA B* **15**, 1192 (1998).

[17] J. Kofler, M. Singh, M. Ebner, M. Keller, M. Kotyrbá, and A. Zeilinger, *Physical Review A* **86**, 032115 (2012).

[18] B. Braverman and C. Simon, *Physical Review Letters* **110**, 060406 (2013).

[19] M. Kaur and M. Singh, *Scientific Reports* **10**, 11427 (2020).

[20] M. Kazemi and V. Hosseinzadeh, *Physical Review A* **107**, 012223 (2023).

[21] C. Gneiting and K. Hornberger, *Physical Review A* **88**, 013610 (2013).

[22] A. Perrin, H. Chang, V. Krachmalnicoff, M. Schellekens, D. Boiron, A. Aspect, and C. I. Westbrook, *Physical review letters* **99**, 150405 (2007).

[23] R. I. Khakimov, B. Henson, D. Shin, S. Hodgman, R. Dall, K. Baldwin, and A. Truscott, *Nature* **540**, 100 (2016).

[24] M. Keller, M. Kotyrbá, F. Leupold, M. Singh, M. Ebner, and A. Zeilinger, *Physical Review A* **90**, 063607 (2014).

[25] C. Kurtsiefer and J. Mlynek, *Applied Physics B* **64**, 85 (1996).

[26] C. Kurtsiefer, T. Pfau, and J. Mlynek, *Nature* **386**, 150 (1997).

[27] In fact, Pauli shows that there is no self-adjoint time operator canonically conjugate to the Hamiltonian if the Hamiltonian spectrum is discrete or has a lower bound [?].

[28] B. Misra and E. G. Sudarshan, *Journal of Mathematical Physics* **18**, 756 (1977).

[29] M. A. Porras, A. Luis, and I. Gonzalo, *Physical Review A* **90**, 062131 (2014).

[30] G. Allcock, *Annals of Physics* **53**, 253 (1969).

[31] B. Mielnik, *Foundations of physics* **24**, 1113 (1994).

[32] C. Leavens, *Physics Letters A* **303**, 154 (2002).

[33] N. Vona, G. Hinrichs, and D. Dürr, *Phys. Rev. Lett.* **111**, 220404 (2013).

[34] D. L. B. Sombillo and E. A. Galapon, *Annals of Physics* **364**, 261 (2016).

[35] S. Das and M. Nöth, *Proceedings of the Royal Society A* **477**, 20210101 (2021).

[36] S. Das and W. Struyve, *Phys. Rev. A* **104**, 042214 (2021).

[37] N. Grot, C. Rovelli, and R. S. Tate, *Physical Review A* **54**, 4676 (1996).

[38] C. Leavens, *Physical Review A* **58**, 840 (1998).

[39] J. Halliwell and E. Zafiris, *Physical Review D* **57**, 3351 (1998).

[40] A. Marchewka and Z. Schuss, *Physical Review A* **65**, 042112 (2002).

[41] E. A. Galapon, R. F. Caballar, and R. T. B. Jr, *Phys. Rev. Lett.* **93**, 180406 (2004).

[42] H. Nitta and T. Kudo, *Phys. Rev. A* **77**, 014102 (2008).

[43] C. Anastopoulos and N. Savvidou, *Physical Review A* **86**, 012111 (2012).

[44] L. Maccone and K. Sacha, *Phys. Rev. Lett.* **124**, 110402 (2020).

[45] S. Roncallo, K. Sacha, and L. Maccone, *Quantum* **7**, 968 (2023).

[46] R. Tumulka, *Phys. Rev. A* **106**, 042220 (2022).

[47] A. A. Rafsanjani, M. Kazemi, A. Bahrampour, and M. Golshani, *arXiv preprint arXiv:2301.02641* (2023).

[48] S. S. Hodgman, W. Bu, S. B. Mann, R. I. Khakimov, and A. G. Truscott, *Physical Review Letters* **122**, 233601 (2019).

[49] M. Brown, S. Muleady, W. Dworschack, R. Lewis-Swan, A. Rey, O. Romero-Isart, and C. Regal, *Nature Physics* **19**, 569 (2023).

[50] S. Das, D.-A. Deckert, L. Kellers, and W. Struyve, *arXiv preprint arXiv:2211.13362* (2022).

[51] J. Bell, *Physics world* **3**, 33 (1990).

[52] S. Goldstein, *Physics Today* **51**, 38 (1998).

[53] A. Benseñy, G. Albareda, Á. S. Sanz, J. Mompart, and X. Oriols, *The European Physical Journal D* **68**, 1 (2014).

[54] D. Dürr, S. Goldstein, and N. Zanghi, *Journal of Statistical Physics* **67**, 843 (1992).

[55] A. Valentini and H. Westman, *Proceedings of the Royal Society A: Mathematical, Physical and Engineering Sciences* **461**, 253 (2005).

[56] D. Bohm, *Phys. Rev.(2)* **85**, 180 (1952).

[57] D. Dürr, S. Goldstein, and N. Zanghi, *Journal of Statistical Physics* **116**, 959 (2004).

[58] J. S. Bell, *International Journal of Quantum Chemistry* **18**, 155 (1980).

[59] S. Das and D. Dürr, *Sci. Rep.* **9**, 2242 (2019).

[60] I. Ivanov, C. H. Nam, and K. T. Kim, *Scientific Reports* **7**, 39919 (2017).

[61] G. Albareda, H. Appel, I. Franco, A. Abedi, and A. Rubio, *Physical review letters* **113**, 083003 (2014).

[62] B. Larder, D. Gericke, S. Richardson, P. Mabey, T. White, and G. Gregori, *Science advances* **5**, eaaw1634 (2019).

[63] Y. Xiao, H. M. Wiseman, J.-S. Xu, Y. Kedem, C.-F. Li, and G.-C. Guo, *Science Advances* **5**, eaav9547 (2019).

[64] J. Foo, E. Asmodelle, A. P. Lund, and T. C. Ralph, *Nature Communications* **13**, 4002 (2022).

[65] T. Zimmerman, S. Mishra, B. R. Doran, D. F. Gordon, and A. S. Landsman, *Physical review letters* **116**, 233603 (2016).

[66] N. Douguet and K. Bartschat, *Physical Review A* **97**, 013402 (2018).

[67] D. Dürr, S. Goldstein, and N. Zanghi, *Studies in History and Philosophy of Science Part B: Studies in History and Philosophy of Modern Physics* **26**, 137 (1995).

[68] D. Dürr, S. Goldstein, and N. Zanghi, *Journal of Statistical Physics* **116**, 959 (2004).

[69] D. Dürr, M. Kolb, T. Moser, and S. Römer, *Letters in Mathematical Physics* **93**, 253 (2010).

[70] T. Norsen and W. Struyve, *Annals of Physics* **350**, 166 (2014).

[71] D. Dürr, S. Goldstein, and N. Zanghi, *Quantum physics without quantum philosophy* (Springer Science & Business Media, 2012).

[72] C. Rovelli, *Foundations of Physics* **52**, 59 (2022).

[73] S. Teufel, D. Dürr, D. Dürr, and S. Teufel, *Bohmian Mechanics* (Springer, 2009).

[74] B. Braverman and C. Simon, *Phys. Rev. Lett.* **110**, 060406 (2013).

[75] D. Georgiev, L. Bello, A. Carmi, and E. Cohen, *Phys. Rev. A* **103**, 062211 (2021).

[76] N. Pathania and T. Qureshi, *Physical Review A* **106**, 012213 (2022).

[77] B. Y. Peled, A. Te'eni, D. Georgiev, E. Cohen, and A. Carmi, *Applied Sciences* **10**, 792 (2020).

[78] A. Sanz, *arXiv preprint arXiv:2306.10104* (2023).

[79] E. Guay and L. Marchildon, *Journal of Physics A: Mathematical and General* **36**, 5617 (2003).

[80] M. Golshani and O. Akhavan, *Journal of Physics A: Mathematical and General* **34**, 5259 (2001).

[81] A. Goussev, *Physical Review A* **91**, 043638 (2015).

[82] K. Akbari, V. Di Giulio, and F. J. García de Abajo, *Science Advances* **8**, eabq2659 (2022).

[83] J.-C. Jaskula, M. Bonneau, G. B. Partridge, V. Krachmalnicoff, P. Deuar, K. V. Kheruntsyan, A. Aspect, D. Boiron, and C. I. Westbrook, *Physical review letters* **105**, 190402 (2010).

[84] The Gaussian solution of the Schrödinger equation for a particle under uniform force was first introduced by de Broglie [?] and rephrased by Holland in [?], but according to our investigation, none of them satisfy the Schrödinger's equation exactly: To satisfying the wave equation, an additional time-dependent phase, i.e. our first exponential term in (6), is needed.

[85] J. Kofler, M. Singh, M. Ebner, M. Keller, M. Kotyra, and A. Zeilinger, *Phys. Rev. A* **86**, 032115 (2012).

[86] A. Perrin, H. Chang, V. Krachmalnicoff, M. Schellekens, D. Boiron, A. Aspect, and C. I. Westbrook, *Phys. Rev. Lett.* **99**, 150405 (2007).

[87] S. Kocsis, B. Braverman, S. Ravets, M. J. Stevens, R. P. Mirin, L. K. Shalm, and A. M. Steinberg, *Science* **332**, 1170 (2011).

[88] D. H. Mahler, L. Rozema, K. Fisher, L. Vermeulen, K. J. Resch, H. M. Wiseman, and A. Steinberg, *Science advances* **2**, e1501466 (2016).

[89] G. Jaeger, M. A. Horne, and A. Shimony, *Physical Review A* **48**, 1023 (1993).

[90] S. Das, M. Nöth, and D. Dürr, *Phys. Rev. A* **99**, 052124 (2019).

[91] C. R. Leavens, *Phys. Rev. A* **58**, 840 (1998).

[92] M. M. Ali, A. S. Majumdar, D. Home, and S. Sengupta, *Phys. Rev. A* **68**, 042105 (2003).

[93] S. V. Mousavi and M. Golshani, *Journal of Physics A: Mathematical and Theoretical* **41**, 375304 (2008).

[94] T. M. Coffey, R. E. Wyatt, and W. C. Schieve, *Phys. Rev. Lett.* **107**, 230403 (2011).

[95] B. Mielnik and G. Torres-Vega, *arXiv preprint arXiv:1112.4198* (2011).

[96] A. Marchewka and Z. Schuss, *Physics Letters A* **240**, 177 (1998).

[97] A. Marchewka and Z. Schuss, *Phys. Rev. A* **61**, 052107 (2000).

[98] A. Marchewka and Z. Schuss, *Phys. Rev. A* **63**, 032108

(2001).

[99] A. Marchewka and Z. Schuss, *Phys. Rev. A* **65**, 042112 (2002).

[100] R. Tumulka, *Communications in Theoretical Physics* (2022).

[101] R. Werner, in *Annales de l'IHP Physique théorique*, Vol. 47 (1987) pp. 429–449.

[102] R. Tumulka, *Annals of Physics* **442**, 168910 (2022).

[103] V. Dubey, C. Bernardin, and A. Dhar, *Phys. Rev. A* **103**, 032221 (2021).

[104] T. Fevens and H. Jiang, *SIAM Journal on Scientific Computing* **21**, 255 (1999).

[105] L. Bulla, M. Pivoluska, K. Hjorth, O. Kohout, J. Lang, S. Ecker, S. P. Neumann, J. Bittermann, R. Kindler, M. Huber, et al., *Physical Review X* **13**, 021001 (2023).

[106] C. Anastopoulos and N. Savvidou, *Physical Review A* **95**, 032105 (2017).

[107] R. Lopes, A. Imanaliev, A. Aspect, M. Cheneau, D. Boiron, and C. I. Westbrook, *Nature* **520**, 66 (2015).

[108] D. S. Shucker, *Journal of Functional Analysis* **38**, 146 (1980).

[109] S. Wolf and H. Helm, *Phys. Rev. A* **62**, 043408 (2000).

[110] E. Wigner, *Phys. Rev.* **40**, 749 (1932).

[111] H.-W. Lee, *Physics Reports* **259**, 147 (1995).

[112] H.-W. Lee, *Foundations of physics* **22**, 995 (1992).

[113] M. Razavy, *Physics Letters A* **212**, 119 (1996).

[114] A. Donoso and C. C. Martens, *Physical Review Letters* **87**, 223202 (2001).

[115] J. Daligault, *Physical Review A* **68**, 010501 (2003).

[116] Y. E. Lozovik, A. Filinov, and A. Arkhipov, *Physical Review E* **67**, 026707 (2003).

[117] L. Wang, C. C. Martens, and Y. Zheng, *The Journal of chemical physics* **137**, 034113 (2012).

[118] O. Steuernagel, D. Kakofengitis, and G. Ritter, *Physical Review Letters* **110**, 030401 (2013).

[119] X. Ren, Y. Wu, L. Wang, and Y. Zheng, *Physics Letters A* **382**, 2662 (2018).

[120] X. Hu, S. Sun, Y. Zheng, et al., *Physical Review A* **101**, 042107 (2020).

[121] Nonetheless, it is worth noting that, since the Wigner function is not positive-definite in general [110], it cannot be interpreted as a realistic phase-space distribution function. Consequently, in contrast to Bohmian trajectories, the Wigner trajectories cannot be reliably utilized to visualize the underlying quantum motion in a completely consistent manner.